Photothermal Analysis of Individual Nanoparticulate Samples Using Micromechanical Resonators

Tom Larsen,[†,‡] Silvan Schmid,[†] Luis G. Villanueva,[†,§] and Anja Boisen[†,*]

[†]Department of Micro- and Nanotechnology, Technical University of Denmark, DTU Nanotech, Building 345 East, DK-2800 Kongens Lyngby, Denmark.
[‡]Present address: Microsystems Laboratory, Stanford University, Stanford, California, U.S.A. [§]Present address: NEMS group, EPFL, Lausanne, Switzerland.

ABSTRACT The ability to detect and analyze single sample entities such as single nanoparticles, viruses, spores, or molecules is of fundamental interest. This can provide insight into the individual specific properties which may differ from the statistical sample average. Here we introduce resonant photothermal spectroscopy, a novel method that enables the analysis of individual nanoparticulate samples. Absorption of light by an individual sample placed on a microstring resonator results in local heating of the string, which is reflected in its resonance frequency. The working principle of the spectrometer is demonstrated by analyzing the optical absorption of different micro- and nanoparticles on a microstring. We present the measurement of a simple absorption spectrum of multiple polystyrene microparticles illuminated with an unfocused LED light source. Using a diode laser, single 170 nm polystyrene nanoparticles are detected. With the current setup, nanoparticulate samples with a mass of ~40 ag are detectable. By using nanostrings, visible and infrared photothermal spectroscopy in the subattogram mass regime is possible and single molecule detection is within reach.

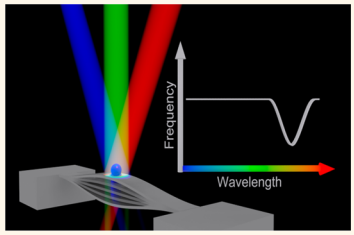

KEYWORDS: nanoparticulate matter · string resonators · photothermal spectroscopy · temperature sensing

Nanoparticulate matter has an impact on our daily life in numerous ways. The exposure to biological materials such as pollen, mold spores, bacteria, viruses, *etc.* can result in allergic reactions or infections which in the worst case can be lethal. In addition to such naturally generated agents, nanoparticulate matter originating from human activities, such as various types of combustion, processing, and synthesis of materials can be extremely toxic.[1]

A lot of effort is currently invested into understanding how nanoparticulate matters are generated and how they interfere with the human organism.[2−5] Of particular interest is the chemical characterization of nanoparticulate samples, which often appear in heterogeneous mixtures. It is therefore necessary to be able to analyze individual samples that may differ from the statistical average of the mixture. Time-consuming and expensive techniques such as scanning electron microscopy (SEM), transmission electron microscopy (TEM), energy-dispersive X-ray spectroscopy (EDX), and mass spectroscopy (MS) are frequently used for this type of analysis.[6,7] An alternative technique is microscale photothermal spectroscopy which is based on wavelength-dependent light absorption by the sample. When the sample is irradiated by light, a fraction of the light is absorbed and transformed into heat which is detected by a thermal sensor. An absorption spectrum can be obtained by sweeping the wavelength of the light while monitoring the generation of heat. If the size of the temperature sensor is small enough, then it is possible to detect minute amounts of absorbed energy. Cantilever-based photothermal spectroscopy has successfully been used to investigate thin films of various kinds and different types of vapors.[8−14] This powerful technique benefits from the low thermal mass that microcantilevers possess. However, the magnitude to be monitored in such experiments (deflection) is directly subjected to thermomechanical noise and external vibrations. In this paper, we present a novel technique called resonant photothermal spectroscopy, where microstrings are used as thermal sensors by monitoring the change in their resonance frequency.[15−17] This apparently subtle modification of the technique (monitoring frequency instead of deflection) allows for a more robust detection scheme, a simpler fabrication (single material structures),

* Address correspondence to anja.boisen@nanotech.dtu.dk.

Received for review April 24, 2013 and accepted June 25, 2013.

Published online June 25, 2013
10.1021/nn402057f

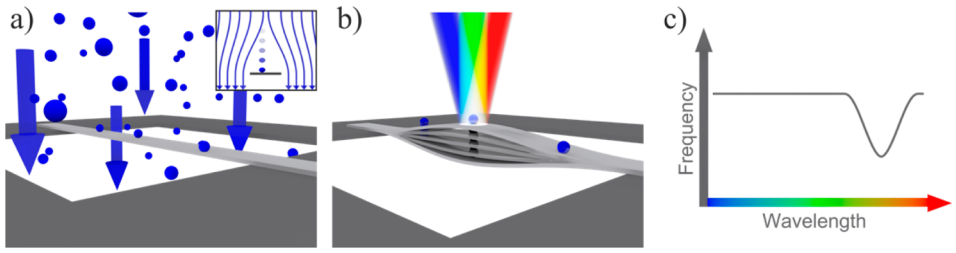

Figure 1. (a) Air stream containing nanoparticulate samples is passed through the hole spanning the string. Due to the high velocity of the air stream, the nanoparticulate matter has enough momentum to leave the air stream, which is bent by the string, and deposit by inertial impaction on the string (see inset). (b) Individual samples deposited on the string are irradiated with light of varying wavelength. A fraction of the absorbed light is converted into thermal energy and conducted into the string which is reflected in its resonance frequency. (c) Characteristic spectrum of the irradiated matter is obtained by plotting the resonance frequency of the string as a function of irradiation wavelength.

reduction in heat dissipation (no metals), and simple analyte sampling.[18] The sampling and detection scheme is illustrated in Figure 1. Typically, diffusion-based sampling of nanoparticulate matter on nanosized sensors is inefficient, which results in long sampling times.[19] We use a non-diffusion-limited sampling method, so-called inertial sampling. The air containing the analyte is flowing through a small opening in the sensor chip. Thereby the analyte is passing the microstring at high velocities at which they are efficiently collected by inertial impaction, as shown in Figure 1a. Once the analyte is captured on the microstring, the photothermal properties of the deposited matter are determined by monitoring the resonance frequency of the string while irradiating individual nanoparticulate samples with light of varying wavelength (Figure 1b,c). We demonstrate the detection and characterization of individual nanoparticulate samples in the attogram mass regime.

Microstring resonators are tensile stressed doubly clamped beams. These structures are described as strings instead of beams as their dynamic behavior is string-like due to the high tensile stress.[20,21] Local heating of a string will make it expand in accordance to its coefficient of thermal expansion. This modifies the tensioning of the string, which is reflected in its resonance frequency.[15−17,22−24] If strings are operated in vacuum, they become excellent temperature sensors for studying thermal processes at the micro- and nanoscale for the following reasons: the strings have low thermal mass; they are well isolated from the surroundings; their time constant is short (∼100 ms); they show incredibly high quality factors ($Q \sim 10^6$),[21,25] and changes in temperature can be measured with a high resolution.[16,17]

In the following, the working principle of the string-based photothermal spectrometer is demonstrated. Different types of micro- and nanoparticles are used as test samples. They are placed on silicon nitride strings and then irradiated with visible light while monitoring the resonance frequency of the strings. The influence of string width, irradiation power and wavelength, and particle type is investigated.

RESULTS AND DISCUSSION

The dynamic properties of the fabricated strings are investigated before placing particles on them. The resonance frequency of the used strings is ∼135 kHz. Higher order resonant modes are multiples of the fundamental one, which is characteristic from string-like behavior. The built-in stress in the constituent silicon nitride has been estimated to be ∼170 MPa by assuming a mass density of 2900 kg/m^3. The quality factor of these structures is around 1 million.[21] The thermal time constant of the strings is measured to be shorter than 250 ms, which is the sampling rate of the frequency counter. The optimum value of the Allan deviation is found for an integration time of few seconds, and it is around 10^{-7}. A relative power responsivity of $-2\%/\mu$W has been estimated for the 3 μm wide strings (180 nm thick, 895 μm long) using finite element simulations. Based on such responsivity estimation and on the obtained Allan Deviation, the detection limit for the 3 μm wide strings is 20 pW when assuming signal-to-noise ratio of 3. The detection limit is less than 1 order of magnitude lower than the one obtained by using more complex bilayer cantilever structures.[26] This is a direct consequence of the larger effect of stress on the resonant frequency of strings, as opposed to cantilevers.[22,27]

Finite element simulations of strings, locally heated at the center, have shown that the induced frequency shift scales with the inverse of the string width and linearly with the absorbed power. Vacuum conditions were simulated by only allowing heat to transfer through radiation and conductions through the anchor regions. Following values have been assumed for the mass density, Young's modulus, Poisson's ratio, coefficient of thermal expansion, specific heat capacity, thermal conductions, and emissivity: 2900 kg/m^3, 250 GPa, 0.23, 10^{-6} K^{-1}, 700 J/(kg·K), 20 W/(m·K), and 1, respectively. The tensile stress matched the one of the fabricated strings.

The influence of string width is investigated experimentally by using the five strings shown in Figure 2a, with blue 2.8 μm polystyrene particles. The relative frequency shift induced when shining a red laser (see Methods) onto the particles and onto the bare

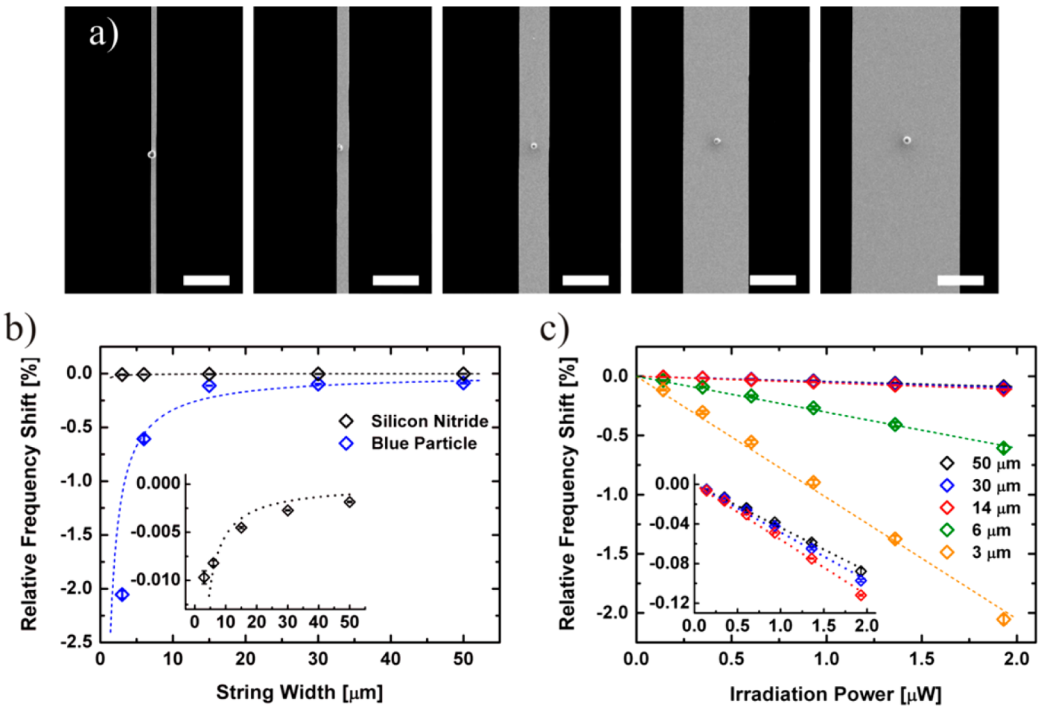

Figure 2. (a) SEM micrographs of silicon nitride strings with a blue polystyrene particle placed at each of the strings' center. The strings are 895 μm long and 180 nm thick. The width, from left to right, is 3, 6, 14, 30, and 50 μm. Scale bars are 20 μm. (b) Induced relative frequency shift when irradiating the strings and the particles on them with a 1.9 μW laser spot, 635 nm, as a function of string width. The size of the laser spot is approximately 6 μm in diameter. The dashed lines represent 1/width fits of the data points. Data points for the 3 μm wide string are omitted in these fits as the laser spot is wider than the string. (c) Induced relative frequency shift as a function of irradiation power when irradiating the particles shown in (a). The dashed lines are linear fits of the data points. The error bars in (b) and (c) represent the standard deviations obtained when repeating the measurements five times.

silicon nitride is shown in Figure 2b. The induced shifts in the two cases can easily be distinguished from each other for all string widths. Hence the added absorption due to the particles can be detected. The magnitude of the shifts is in both cases increasing for decreasing string width, which is in accordance with the simulations described above.

Simulations predict a linear relation between relative frequency shift and irradiation power, which is tested using the same strings (see Figure 2c). The relative frequency shift is proportional to the irradiation power in all cases. This is true both when irradiating the blue particles (Figure 2c) and when irradiating the bare silicon nitride (data not shown). The relative frequency shift induced when irradiating the particle and the string it is placed on can easily be distinguished from each other for all string widths and power levels. The influence of the string width can also be seen in the plot.

From these experiments, it is clear that the added light absorption due to the presence of a single particle on a string can be detected. The next step is to demonstrate that dissimilar light absorption by different types of particles can be used to distinguish them from each other. Light absorption by a blue, brown, and white particle placed on a string has been investigated by using the string and particles shown in Figure 3a. The relative frequency shift induced when irradiating—with the red laser—the bare silicon nitride and the three particles individually is plotted as a function of irradiation power in Figure 3b. The shifts induced in the four cases can be distinguished from each other for all power levels. The magnitude of the induced shifts when irradiating the particles can be correlated to their respective colors. A blue particle is expected to absorb more red light than a brown particle, which is again expected to absorb more light than a white particle. A linear relation between relative frequency shift and irradiation power is observed in all four cases, following the trend shown in Figure 2c.

The frequency shift induced when irradiating a particle will depend not only on the nature of the particle and the sensitivity of the string but also on the size of the particle and the size/intensity of the light spot used to irradiate it. Two situations can appear, one in which the light spot is smaller than the particle and another where the opposite is the case. In the first situation, the induced frequency shift is to a rough estimation independent of the size of the particle. In the second situation, which is the case in these studies, the induced frequency shift is dependent on the size of the particle. The magnitude of the shift will decrease with decreasing particle size. The data presented in Figure 3b are therefore a convolution of two effects:

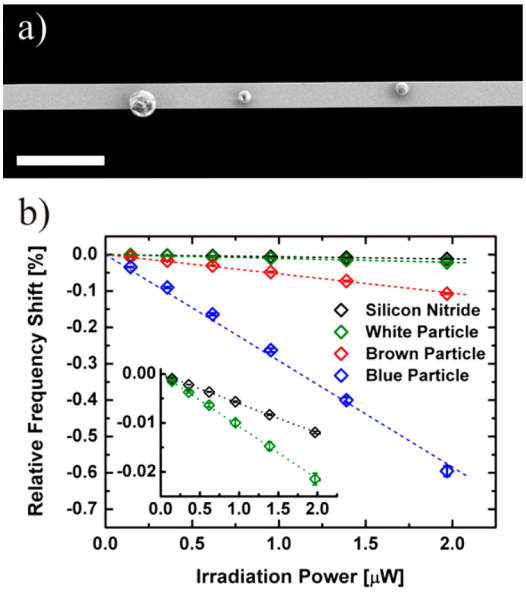

Figure 3. (a) SEM micrograph of a 917 μm long, 6 μm wide, and 180 nm thick silicon nitride string with a white polystyrene (left), blue polystyrene (middle), and brown (right) particle placed on it. The scale bar has a length of 20 μm. (b) Induced relative frequency shift when irradiating the three particles and the string in (a) as a function of irradiation power. The dashed lines are linear fits of the data points. The wavelength of the irradiation light is 635 nm, and the spot size is ~6 μm. The error bars represent the standard deviations obtained when repeating the measurements five times.

particles size and color. However, the blue and brown particles are similar in size, and they are both smaller than the white particle. Therefore, the size of the particles does not change the quantitative results of the experiment. A situation where the difference in size of two particles could dominate over the different nature of them is likely to take place. This problem can be circumvented by irradiating the two particles with light of different wavelengths. The wavelength-dependent absorption can then be used to distinguish them from each other based on their photothermal properties and not their size. This is the basic foundation of photothermal resonant spectroscopy, as demonstrated below.

Wavelength-dependent absorption by blue polystyrene particles is investigated by placing ~30 blue microparticles on a string and then irradiating them with red, green, and blue LED light (see Methods). A string without any particles is used as a reference string as the position of the LEDs is fixed. The power of the red, green, and blue light beam after passing a 221 μm × 528 μm slide is ~4, ~11, and ~7 μW, respectively. The difference in induced frequency shift when irradiating the two strings is plotted in Figure 4. The pattern seen in Figure 4 can be correlated to the color of the particles. Hence, Figure 4 presents the red–green–blue absorption spectrum of blue microparticles. A more detailed absorption spectrum can be obtained by performing a finer sweep of the wavelength of monochromatic light. By using infrared

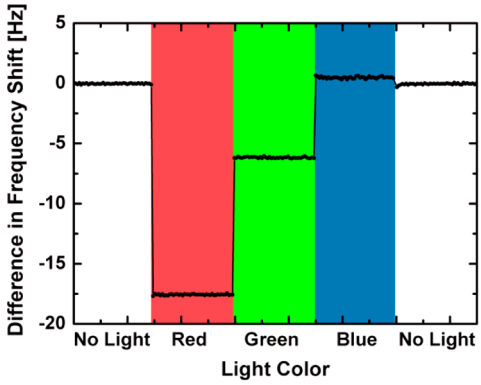

Figure 4. RGB absorption spectrum of blue polystyrene microparticles. Approximately 30 blue polystyrene microparticles are placed on a 917 μm long, 30 μm wide, and 180 nm thick string and then irradiated with red, green, and blue LED light. The *y*-axis represents the difference in induced frequency shift between a string with particles and an empty reference.

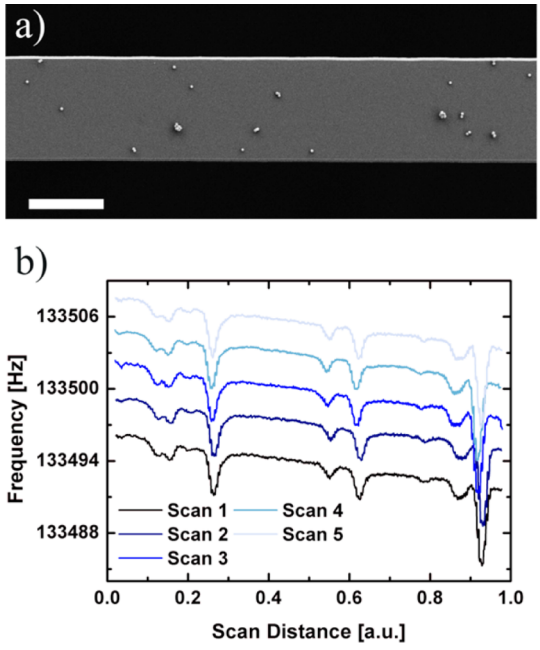

Figure 5. (a) SEM picture of a string with 170 nm blue polystyrene particles deposited onto it. The scale bar has a length of 4 μm. (b) Measured resonance frequency of an 897 μm long, 6 μm wide, and 180 nm thick string with blue polystyrene nanoparticles when scanning a 1.5 μW red (635 nm) laser beam along it.

light, information about the chemical structure of the sample can be obtained.[11–13,28]

Micrometer-sized particles have been used in the experiments described so far. To demonstrate that true nanoparticulate samples can be detected, 170 nm blue polystyrene particles are first deposited on a string (see Methods) and then irradiated by light from the red laser diode. A SEM micrograph of a string with particles can be seen in Figure 5a. The measured resonance frequency of such string when scanning the laser beam along it can be seen in Figure 5b. The same scan

is repeated five times. The resonance frequency is shifted upward from scan to scan due to temperature drift inside the vacuum chamber. The drift is visible because the laser light is not chopped in these measurements. The scan direction is toward the center of the string, which explains the negative slope of the curves' baselines. A number of peaks can be identified in the scans. Assuming that the power distribution of the heating laser is uniform, and given that the particle size is well-determined, the size of the peaks should be related to the number of particles irradiated. Therefore, considering that the smallest peak is due to the irradiation of a single particle, we can estimate the ratios from the larger peaks to the allegedly single particle. Using this approach, the ratios are 2.0 ± 0.2, 2.1 ± 0.2, 3.1 ± 0.4, 3.3 ± 0.3, 4.1 ± 0.2, 8.0 ± 0.4, and 9.7 ± 0.7, where the error is calculated from the standard deviation of the five different scans that were performed in this experiment. All frequency shifts have been corrected accounting for position-dependent sensitivity and temperature drift in the measurements. The presented measurements show that nanoparticulate samples can be detected.

The amount of light absorbed by a sample in most cases decreases with decreasing sample size. If it is assumed that the absorption of light increases linearly with the surface area irradiated, the minimum detectable sample size can be estimated. The estimated lower limit for the blue polystyrene particles is particles with a diameter ~40 nm having a mass of ~40 ag, where we assume that a particle is detectable when it induces a relative shift that equals three times the Allan deviation ($3\sigma(1s) \approx 4.8 \times 10^{-7}$) obtained for the 6 μm wide strings. The relative frequency shift induced per unit area irradiated is estimated from the relative shift induced by the 2.8 μm and 170 nm particles when irradiating them with a ~1.5 μW red laser spot.

As we describe in Figure 2, the relative frequency shift can be maximized by reducing string width and increasing irradiation power. It is also expected that a reduction in the string thickness will have a positive effect on the induced frequency shift. The heat transfer to the two anchor regions will be reduced in a similar way as when the string width is reduced. By using a thinner and narrower string, subattogram samples should be detectable.

CONCLUSIONS

As a summary, we successfully demonstrate that the added absorption of light due to the presence of a nanoparticulate sample can be used to detect and identify the sample. Simulations and experimental results have shown that the induced frequency shift increases for decreasing string width and increasing irradiation power. Three different types of samples could be distinguished from each other based on their different photothermal properties. Detection of wavelength-dependent absorption was demonstrated by irradiating blue polystyrene particles with red, green, and blue light. Finally, it was proven that samples with a mass of 3 fg can be detected. It have been estimated that single blue polystyrene nanoparticles with a mass of ~40 ag can be detected with the currently used setup. With an improved setup, visible and infrared photothermal spectroscopy of subattogram samples should be within reach.

METHODS

The silicon nitride strings used in the experiments are fabricated by standard surface and bulk micromachining. LPCVD (low-pressure chemical vapor deposition) silicon-rich silicon nitride is deposited on a 350 μm thick double-side-polished silicon wafer. The strings are then defined on the front side by reactive ion etching. A protective PECVD (plasma-enhanced chemical vapor deposition) silicon nitride layer is deposited on top of the structured LPCVD silicon nitride. The backside silicon nitride is patterned by reactive ion etching, opening windows for the subsequent release step, which is achieved through a standard potassium hydroxide etch. The protective PECVD silicon nitride layer is then removed in buffered hydrofluoric acid. The fabricated strings have a thickness of 180 nm, a length of 895−917 μm, and a width of 3, 6, 14, 30, or 50 μm.

Four different types of particles are used in the experiments: blue polystyrene particles with a diameter and mass of 2.8 μm and 12 pg, respectively (68553, Sigma Aldrich); blue polystyrene nanoparticles (170 nm and 3 fg; 15706-15, Polysciences GmbH); brown particles (2.8 μm and 15 pg; M280, Dynabeads); and white polystyrene particles (5.9 μm and 114 pg; 07312, Polybeads). An etched tungsten needle with a tip diameter of roughly 1 μm placed on a high-precision *xyz* stage is used to manually pick the microparticles and place them on the strings.[29] The 170 nm nanoparticles are deposited on the strings by the previously discussed inertial sampling method.[18]

The analyzed strings are actuated with a piezo element, and the mechanical vibration is read out using a laser-Doppler vibrometer (MSA-500, Polytec GmbH). The strings are operated in a positive feedback loop at the fundamental harmonic, and the oscillation frequency is monitored with a frequency counter (53132A, Agilent Technologies). The irradiation experiments are performed with four different types of light sources: a 635 nm laser diode (L635P005, Thorlabs) with a spot diameter of ~6 μm; and red (625 nm), green (525 nm), and blue (460 nm) LEDs (F50360, Soul Semiconductor) passed through a 221 μm × 528 μm slide. Both laser and LEDs are electrically chopped with a frequency of 1 and 0.5 Hz, respectively, to reduce the influence of background temperature drift. The strings are kept at a pressure below 10^{-5} mbar during the measurements.

Conflict of Interest: The authors declare no competing financial interest.

Acknowledgment. The authors would like to thank Shoko Yamada for the helpful discussions. This research was supported by the Villum Kann Rasmussen Centre of Excellence "NAMEC" under Contract No. 65286. S.S. acknowledges financial support from the European Commission (EuropeanCommunity's Seventh Framework Programme(FP7/2007-2013) under Grant Agreement No. 211464-2). L.G.V. acknowledges financial support from the European Commission (PIOF-GA-2008-220682).

REFERENCES AND NOTES

1. Buzea, C.; Pacheco, I. I.; Robbie, K. Nanomaterials and Nanoparticles: Sources and Toxicity. *Biointerphases* **2007**, *2*, 17–172.

2. Mauderly, J. L.; Chow, J. C. Health Effects of Organic Aerosols. *Inhalation Toxicol.* **2008**, *20*, 257–288.
3. Nel, A.; Xia, T.; Mädler, L.; Li, N. Toxic Potential of Materials at the Nanolevel. *Science* **2006**, *311*, 622–627.
4. Nel, A. E.; Mädler, L.; Velegol, D.; Xia, T.; Hoek, E. M.; Somasundaran, P.; Klaessig, F.; Castranova, V.; Thompson, M. Understanding Biophysicochemical Interactions at the Nano–Bio Interface. *Nat. Mater.* **2009**, *8*, 543–557.
5. Auffan, M.; Rose, J.; Bottero, J. Y.; Lowry, G. V.; Jolivet, J. P.; Wiesner, M. R. Towards a Definition of Inorganic Nanoparticles from an Environmental, Health and Safety Perspective. *Nat. Nanotechnol.* **2009**, *4*, 634–641.
6. Marquis, B. J.; Love, S. A.; Braun, K. L.; Haynes, C. L. Analytical Methods To Assess Nanoparticle Toxicity. *Analyst* **2009**, *134*, 425–439.
7. Kuhlbusch, T.; Asbach, C.; Fissan, H.; Göhler, D.; Stinzt, M. Nanoparticle Exposure at Nanotechnology Workplaces: A Review. *Part. Fibre Toxicol.* **2011**, *8*, 22.
8. Barnes, J. R.; Stephenson, R. J.; Woodburn, C. N.; Oshea, S. J.; Welland, M. E.; Rayment, T.; Gimzewski, J. K.; Gerber, C. A Femtojoule Calorimeter Using Micromechanical Sensors. *Rev. Sci. Instrum.* **1994**, *65*, 3793–3798.
9. Barnes, J. R.; Stephenson, R. J.; Welland, M. E.; Gerber, C.; Gimzewski, J. K. Photothermal Spectroscopy with Femtojoule Sensitivity Using a Micromechanical Device. *Nature* **1994**, *372*, 79–81.
10. Datskos, P. G.; Sepaniak, M. J.; Tipple, C. A.; Lavrik, N. Photomechanical Chemical Microsensors. *Sens. Actuators, B* **2001**, *76*, 393–402.
11. Wig, A.; Arakawa, E. T.; Passian, A.; Ferrell, T. L.; Thundat, T. Photothermal Spectroscopy of *Bacillus anthracis* and *Bacillus cereus* with Microcantilevers. *Sens. Actuators, B* **2006**, *114*, 206–211.
12. Krause, A. R.; Van Neste, C.; Senesac, L.; Thundat, T.; Finot, E. Trace Explosive Detection Using Photothermal Deflection Spectroscopy. *J. Appl. Phys.* **2008**, *103*, 094906.
13. Yun, M.; Kim, S.; Lee, D.; Jung, N.; Chae, I.; Jeon, S.; Thundat, T. Photothermal Cantilever Deflection Spectroscopy of a Photosensitive Polymer. *Appl. Phys. Lett.* **2012**, *100*, 204103.
14. Finot, E.; Rouger, V.; Markey, L.; Seigneuric, R.; Nadal, M. H.; Thundat, T. Visible Photothermal Deflection Spectroscopy Using Microcantilevers. *Sens. Actuators, B* **2012**, *169*, 222–228.
15. Pandey, A. K.; Gottlieb, O.; Shtempluck, O.; Buks, E. Performance of an AuPd Micromechanical Resonator as a Temperature Sensor. *Appl. Phys. Lett.* **2010**, *96*, 203105.
16. Larsen, T.; Schmid, S.; Grönberg, L.; Niskanen, A. O.; Hassel, J.; Dohn, S.; Boisen, A. Ultrasensitive String-Based Temperature Sensors. *Appl. Phys. Lett.* **2011**, *98*, 121901.
17. Larsen, T.; Schmid, S.; Boisen, A. Micro String Resonators as Temperature Sensors. *Temp.: Its Meas. Control Sci. Ind.* **2013**, in press.
18. Schmid, S.; Kurek, M.; Adolphsen, J. Q.; Boisen, A. Real-Time Single Airborne Nanoparticle Detection with Nanomechanical Resonant Filter-Fiber. *Sci. Rep.* **2013**, *3*, 1288.
19. Squires, T. M.; Messinger, R. J.; Manalis, S. R. Making it Stick: Convection, Reaction and Diffusion in Surface-Based Biosensors. *Nat. Biotechnol.* **2008**, *26*, 417–426.
20. Schmid, S.; Dohn, S.; Boisen, A. Real-Time Particle Mass Spectrometry Based on Resonant Micro Strings. *Sensors* **2010**, *10*, 8092–8100.
21. Schmid, S.; Jensen, K. D.; Nielsen, K. H.; Boisen, A. Damping Mechanisms in High-Q Micro and Nanomechanical String Resonators. *Phys. Rev. B: Condens. Matter Mater. Phys.* **2011**, *84*, 165307.
22. Karabalin, R. B.; Villanueva, L. G.; Matheny, M. H.; Sader, J. E.; Roukes, M. L. Stress-Induced Variations in the Stiffness of Micro- and Nanocantilever Beams. *Phys. Rev. Lett.* **2012**, *108*, 236101.
23. Henriksson, J. G.; Villanueva, L. G.; Brugger, J. Ultra-Low Power Hydrogen Sensing Based on a Palladium-Coated Nanomechanical Beam Resonator. *Nanoscale* **2012**, *4*, 5059–5064.
24. Zhang, X.; Myers, E. B.; Sader, J. E.; Roukes, M. L. Nanomechanical Torsional Resonators for Frequency-Shift Infrared Thermal Sensing. *Nano Lett.* **2013**, *13*, 1528–1534.
25. Verbridge, S. S.; Craighead, H. G.; Parpia, J. M. A Megahertz Nanomechanical Resonator with Room Temperature Quality Factor over a Million. *Appl. Phys. Lett.* **2008**, *92*, 013112.
26. Sadat, S.; Chua, Y. J.; Lee, W.; Ganjeh, Y.; Kurabayashi, K.; Meyhofer, E.; Reddy, P. Room Temperature Picowatt-Resolution Calorimetry. *Appl. Phys. Lett.* **2011**, *99*, 043106.
27. Pini, V.; Tamayo, J.; Gil-Santos, E.; Ramos, D.; Kosaka, P.; Tong, H. D.; Rijn, C. V.; Calleja, M. Shedding Light on Axial Stress Effect on Resonance Frequencies of Nanocantilevers. *ACS Nano* **2011**, *5*, 4269–4275.
28. Griffiths, P.; De Haseth, J. A. *Fourier Transform Infrared Spectrometry*, John Wiley & Sons: Hoboken, NJ, 2007; Vol. 171.
29. Dohn, S.; Sandberg, R.; Svendsen, W.; Boisen, A. Enhanced Functionality of Cantilever Based Mass Sensors Using Higher Modes. *Appl. Phys. Lett.* **2005**, *86*, 233501.